Check for updates

Limonin alleviates high-fat diet-induced dyslipidemia by regulating the intestinal barrier *via* the microbiota-related ILC3–IL22–IL22R pathway†

Wangling Wu, [ID] Yingying Pan, Tianyan Zheng, Haoyi Sun, Xia Li, Haiyan Zhu, Zheng Wang and Xin Zhou*

High-fat diet (HFD)-induced dyslipidemia is frequently accompanied by gut microbiota dysbiosis and a compromised gut barrier. Enhancing the intestinal barrier function emerges as a potential therapeutic approach for dyslipidemia. The ILC3–IL22–IL22R pathway, which responds to dietary and microbial signals, has not only attracted attention for its crucial role in maintaining the intestinal barrier, but recent reports have also suggested its potential in regulating lipid metabolism. Limonin is derived from the Chinese herb *Evodiae fructus*, which has shown potential in ameliorating dysbiosis of serum lipids. However, its underlying mechanisms remain elusive. Consequently, targeting the ILC3–IL22–IL22R pathway to enhance intestinal barrier function holds promise as a therapeutic approach for dyslipidemia. In this study, male C57BL/6 mice were subjected to a 16-week HFD to induce dyslipidemia and concurrently administered oral limonin. We discovered that limonin supplementation dramatically reduced serum lipid profiles in HFD-fed mice, significantly curbing HFD-induced weight gain and epididymal fat accumulation. Ileal histopathological evaluation indicated limonin's ameliorative effects on HFD-induced intestinal barrier impairment. Limonin also moderated the intestinal microbiota dysbiosis, which is characterized by the elevation of Firmicutes in HFD mice, and notably amplified the abundance of probiotic *Lactobacillus*. In addition, supported by flow cytometry and other analyses, we observed that limonin upregulated the ILC3–IL22–IL22R pathway, enhancing phosphorylated STAT3 (pSTAT3) in intestinal epithelial cells (IECs), thereby reducing lipid transporter expression. In conclusion, our study revealed that limonin exerted a promising preventive effect against HFD-induced dyslipidemia by the mitigation of the intestinal barrier function and intestinal microbiota, and its mechanism was related to the upregulation of the ILC3–IL22–IL22R pathway.

Introduction

Dyslipidemia is a general term that encompasses all disorders of lipid metabolism, mainly referring to the increased plasma concentrations of total cholesterol (TC), triglycerides (TG) or low-density lipoprotein cholesterol (LDL-C), or the decreased plasma concentrations of high-density lipoprotein cholesterol (HDL-C) or a combination of these characteristics.[1] Crucially, dyslipidemia stands as a significant risk factor for ischemic heart disease (IHD), one of the leading causes of global mortality.[2] In 2019, ~4.40 million deaths and ~98.62 million disability-adjusted life years (DALYs) were attributable to high plasma LDL-C levels.[3] The 2017 Global Burden of Disease

Study (GBD) suggested that socioeconomic development and the ubiquitous "Western" high-sugar and high-fat diet intake are considered the main reasons for the increase in plasma lipid levels, while high plasma LDL-C levels are one of the main risk factors for all-cause risk attributable burden in 2017.[4] While the extensive use of statins in high-income countries has significantly decreased plasma LDL-C levels and cardiovascular disease-related deaths,[5] their accessibility remains limited in low-income countries.[6] Consequently, dyslipidemia continues to be an underdiagnosed and undertreated condition globally.[2]

Numerous studies have reported that the consumption of HFD contributed to gut microbiota dysbiosis and intestinal barrier function impairment.[7,8] The intestinal barrier consists of intestinal epithelial cells and immune cells.[9] When dietary lipids are digested in the lumen, they are transported into the enterocytes through specialized lipid transporters.[10] Therefore, intestinal barrier integrity and functional homeostasis provide

School of Basic Medicine, Chengdu University of Traditional Chinese Medicine, Chengdu, 611137, China. E-mail: zhouxin@cdutcm.edu.cn

an important guarantee for appropriate lipid metabolism. Group 3 innate lymphoid cells (ILC3s) are one of the novel populations of innate lymphoid cells (ILCs), most of which are concentrated in the intestinal lamina propria and mucosal tissue, and participate in maintaining epithelial integrity and barrier function.[11,12] Intestinal ILC3s are characterized by the expression of RORγt[+] and interleukin (IL)-22.[13] They can integrate environmental signals, including diet and microbiota, to stimulate the production of IL-22.[14] Specifically, the gut microbiota and metabolites can enhance ILC3s through the aryl hydrocarbon receptor (AhR) pathway,[15] as well as regulate the functional response of ILC3s through toll-like receptor (TLR) signaling,[14] leading to the production of IL-22. IL-22 binds to the IL-22 receptor (IL-22R) expressed in IECs, activating the STAT3 transduction pathway, and stimulating the production of intestinal antimicrobial peptides (RegIIIβ and RegIIIγ), thereby promoting the intestinal barrier.[16–18] Recently, studies have shown that the ILC3-IL22 pathway can modulate intestinal lipid transporters, thereby reshaping host lipid metabolism in the absence of adaptive CD4^{+} T-cells.[19] Supplementation with dietary fiber has been shown to induce IL-22 in a microbiota-dependent manner, thereby protecting HFD-induced metabolic syndrome.[20] What remains unequivocal is that the ILC3–IL22–IL22R pathway is not only solely linked to the intestinal barrier but also deeply intertwined with host metabolism. Furthermore, the gut microbiota plays a crucial role in regulating gut lipid metabolism and the gut barrier.[9,21–23] The gut microbiota can convert complex carbohydrates and sugars into short-chain fatty acids (SCFAs), orchestrating the host energy balance.[24] Certain intestinal microbiota, such as *Lactobacillus* and *Bifidobacterium*, have been shown to promote the intestinal barrier function.[25,26] In conclusion, the ILC3–IL22–IL22R pathway, which is influenced by the gut microbiota, can ameliorate intestinal barrier impairment and represents a potential therapeutic target for HFD-induced dyslipidemia.

Limonin (Fig. 1A), also known as evodin, is a natural tetracyclic triterpenoid compound that widely exists in the traditional Chinese herb *Evodiae fructus* and citrus fruits, and exhibits extensive pharmacological effects, including anti-cancer, anti-inflammatory, anti-bacterial, anti-viral, anti-oxidant, anti-obesity, and hepatoprotective effects *etc*.[27] Limonin has low solubility, poor oral absorption, and low bioavailability, and a large portion of oral limonin is not absorbed and persists in the gut, which may lead to alterations in the gut microbiota.[27,28] Research has demonstrated that limonin therapy significantly enriched Bacteroidetes while inhibiting Firmicutes, and considerably boosted the abundance of the genus *Oscillospira* to lower incidence of inflammatory bowel disease and leanness in humans.[28] Limonin also ameliorated indomethacin-induced intestinal damage and ulcers.[29] Noteworthily, limonin significantly reduced serum TC and TG levels in obese mice[30] and diminished the accumulation of lipid droplets in the liver, in addition to downregulating the levels of lipogenic transcription factors FASN and SREBP1 in non-alcoholic fatty liver disease (NAFLD).[31] Yet, it remains unclear whether limonin's improvement of dyslipidemia is

related to the regulation of the gut barrier and gut microbiota. Therefore, the purpose of this study was to investigate whether the anti-dyslipidemic effect of limonin is related to the intestinal barrier and intestinal microbiota and to explore its mechanism based on the ILC3–IL22–IL22R pathway.

In this study, we utilized C57BL/6 mice subjected to a high-fat diet, mimicking the western high-fat diet pattern, to investigate the underlying mechanism of limonin in improving HFD-induced dyslipidemia. 16S rRNA gene sequencing was used to investigate the composition of the gut microbiota. Then, the proportion of RORγt[+] ILC3s was analyzed by flow cytometry. By using immunofluorescence and quantitative reverse transcription polymerase chain reaction (qRT-PCR), we further determined the levels of molecules connected to the ILC3–IL22–IL22R pathway. We also used western blot to detect the lipid transporter levels. In addition, we comprehensively analyzed the relationship between specific intestinal microbiota and intestinal barrier function biomarkers, to explore the molecular mechanism of limonin against HFD-induced dyslipidemia based on the ILC3–IL22–IL22R pathway.

Materials and methods

Drugs and reagents

Limonin (Lim, 98% purity, S31594) was obtained from Shanghai Yuanye Bio-Technology Co., Ltd (Shanghai, China). Sodium carboxymethyl cellulose (CMC-Na) was obtained from Sigma-Aldrich (St Louis, MO, USA). Isoflurane (R510-22-10) was purchased from Reward Life Technology Co., Ltd (Shenzhen, China). RPMI-1640 and Dulbecco's modified Eagle's medium (DMEM) were purchased from Gibco (Grand Island, USA). Fetal bovine serum (FBS, 04-001-1A) was purchased from Biological Industries (Beit Haemek, Israel). D-Hanks (HBSS, H1040), HEPES (H8090), EDTA (E1170), DTT (D1070), penicillin–streptomycin (P1400), 1× PBS (P1020), 10× PBS (P1022), Percoll (P8370) and DNase I (D8071) were purchased from Beijing Solarbio Science & Technology Co., Ltd (Beijing, China). FVS510 (564406), lineage antibody cocktail (561317), transcription factor buffer set (562574), 70 μM cell strainer (352350), and antibodies against CD16/CD32 (553141), CD127 (A7R34), CD45 (557659) and RORγt (562894) were purchased from BD Pharmingen (Santiago, Chile) and eBioscience (Waltham, USA). Liberase TL (05401020001) was purchased from Roche (Basel, Switzerland). IL-22 Rα1 antibody (MAB42941) was purchased from R&D Systems (Minnesota, USA). RORG (DF3196) was purchased from Affinity Bioscience (Changzhou, China). pSTAT3 antibody (#9145T) was purchased from Cell Signaling Technology (Beverly, USA). ZO-1 and occludin antibodies were purchased from Wuhan Servicebio Technology Co., Ltd (Wuhan, China). Animal total RNA isolation kit (RE-03011) was purchased from Foregene Co., Ltd (Chengdu, China). HiScript III All-in-one RT SuperMix Perfect for qPCR (R333) was purchased from Vazyme Biotech Co., Ltd (Nanjing, China). TAKARA TB Green Premix Ex Taq II (RR820A) was purchased from Takara Biomedical Technology (Beijing)
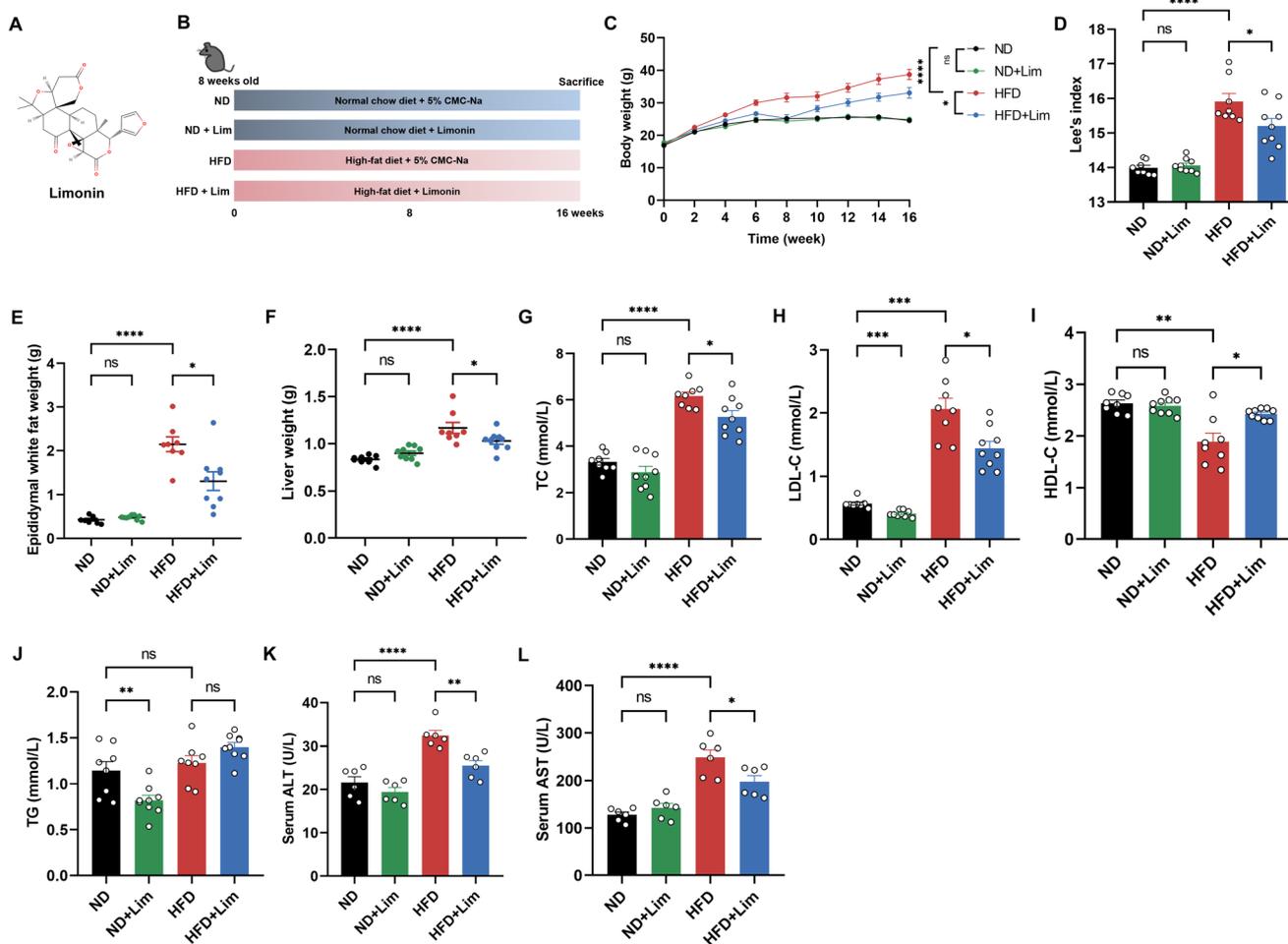
Fig. 1 Limonin improved HFD-induced dyslipidemia. (A) The chemical structure of limonin. (B) Experimental design for dietary and limonin treatment in C57BL/6 mice. (C) Body weight changes during the experiments. (D) Lee's index comparison among ND, ND + Lim, HFD, and HFD + Lim groups. (E) Epididymal white fat weight, and (F) liver weight. Serum lipid profiles of (G) total cholesterol (TC), (H) low-density lipoprotein cholesterol (LDL-C), (I) high-density lipoprotein cholesterol (HDL-C), (J) and triglycerides (TG). All data were expressed as mean $\pm$ SEM (n = 8 for ND and HFD, n = 9 for ND + Lim and HFD + Lim). Serum levels of (K) alanine aminotransferase (ALT) and (L) aspartate aminotransferase (AST). All data were expressed as mean $\pm$ SEM with 6 samples in each group. *$p < 0.05$; ** $p < 0.01$; *** $p < 0.001$; **** $p < 0.0001$.

Co., Ltd (Beijing, China). PIPA lysis buffer (PC101) and ECL kit (SQ201) were purchased from Epizyme Biotech Co., Ltd (Shanghai, China). The antibody against NPC1L1 (sc-166802) was obtained from Santa Cruz Biotechnology Inc., (Texas, USA). The antibody against CD36 (ab252923) was obtained from Abcam (Shanghai) Trading Co., Ltd, (Shanghai, China). β-Tubulin (A01857-1) was purchased from Boster Biological Technology Co. Ltd (Wuhan, China).

Animals and experimental design

Male C57BL/6 mice (8 weeks), weighing 16–19 g, were purchased from Beijing HFK Biotechnology Co., Ltd (Beijing, China; certification no. SCXK-JING 2019-0008). All animals were maintained at standard temperature (22 ± 2 °C), and humidity (55% ± 2%) with controlled light conditions (12 h of light/dark cycle). All mice had access to water and food.

The animal study was performed in strict accordance with the Guidelines for the Care and Use of Laboratory Animals of

the Ministry of Science and Technology of China and was authorized by the Ethics Committee of Chengdu University of Traditional Chinese Medicine (Chengdu, China) with approval number 2021DL-001.

The overview of the experimental design is illustrated in Fig. 1B. After one week of acclimation, all animals were randomly divided into four groups including the normal diet (ND) group (n = 8), ND + Lim group (n = 9), HFD group (n = 8), and HFD + Lim group (n = 9). During the experimental period, ND and ND + Lim groups were fed a normal diet (containing 14.7 kcal% protein, 75.9 kcal% carbohydrate and 9.4 kcal% fat, Research Diets D10012M, Research Diets, NJ), while HFD and HFD + Lim groups were fed a high-fat diet (containing 20 kcal% protein, 20 kcal% carbohydrate and 60 kcal% fat, Research Diets D12492, Research Diets, NJ). Both the ND + Lim group and HFD + Lim group were orally administered with limonin (Lim, 50 mg per kg per day) dissolved in 0.5% CMC-Na, while the ND group and HFD group were orally admi-

nistered with 0.5% CMC-Na as vehicle control. Dietary and limonin interventions were administered simultaneously for 16 weeks.

Body weight and serum lipid profiles were monitored weekly. At the end of the study, fecal samples were collected, and then the mice were anesthetized with isoflurane and sacrificed. Blood collection was performed by extruding the mice's eyeballs and then centrifuging at 3500g and 4 °C for 10 min to obtain the serum. Intestinal tissue, epididymal white adipose, and liver tissue were collected after sacrifice. Body mass index was calculated using Lee's index and the formula used was [body weight (g) × 1000/body length (cm)]$^{1/3}$.

Biochemical parameter analysis

The serum levels of total cholesterol (TC, A111-1-1), triglyceride (TG, A110-1-1), high-density lipoprotein cholesterol (HDL-C, A112-1-1), and low-density lipoprotein cholesterol (LDL-C, A113-1-1) were detected using biochemical kits (Nanjing Jiancheng Bioengineering Institute, Nanjing, China) according to the product instructions. Aspartate aminotransferase (AST, 105-000443-00) and alanine aminotransferase (ALT, 105-000442-00) were purchased from Mindray Bio-medical Electronics Company (Mindray Bio-medical Electronics Company, Ltd, Shenzhen, China) and the serum ALT and AST were measured using a fully automatic biochemical analyzer (BS-240VET, Mindray Bio-medical Electronics Company, Ltd, Shenzhen, China).

Extraction of intestinal lamina propria lymphocytes and flow cytometry analysis

The intestinal lamina propria was extracted according to the protocol proposed by Xiaohuan Guo et al.[11] Specifically, the mice were sacrificed and the small intestine was excised and transferred to ice-cold PBS. The mesenteric material fat and Peyer's patches were carefully removed. The intestines were cut longitudinally, rinsed thoroughly with PBS, and cut into 1 cm pieces. The tissue was incubated in HBSS (without Ca^{2+} and Mg^{2+}) containing 3% FBS, 1 mM DTT, 5 mM EDTA, and 10 mM HEPES at 37 °C for 20 min and subsequently washed with HBSS (without Ca^{2+} and Mg^{2+}) containing 10 mM HEPES at 37 °C for 20 min. Then the tissue was digested in RPMI-1640 containing 10 mM HEPES, 100 U mL^{-1} penicillin–streptomycin, Liberase TL (Roche) (0.1 mg mL^{-1}), and DNase I (20 μg mL^{-1}) at 37 °C for 20 min with slow rotation. 5 mL of RPMI-1640 containing 10 mM HEPES, 100 U mL^{-1} penicillin–streptomycin and 3% FBS was added to terminate the digestion, and then the sample suspension was filtered by using a 70 μm cell strainer. Finally, the sample suspension was centrifuged at 300g for 7 min at 4 °C. The cells were resuspended in 4 mL of medium containing DMEM, 10 mM HEPES, 100 U mL^{-1} penicillin–streptomycin and 3% FBS after discarding the supernatant completely. The single-cell suspension was harvested from the interphase of an 80% and 40% Percoll gradient after a spin at 1000g for 20 min at 4 °C. The middle lymphocyte layer was carefully collected, rinsed with ice-cold PBS, and centrifuged at 800g for 10 min at 4 °C, then resuspended in ice-cold PBS for cell staining. Firstly, the cell was incubated with 1 μL mL^{-1} fixable viability stain 510 on ice for 30 min to gate out dead cells and then washed with FACS buffer by centrifugation at 350g for 5 min at 4 °C. Secondly, the cells were resuspended in FACS buffer containing anti-mouse CD16/CD32 at a concentration of 1 μL/100 μL to block Fc receptor internalization. Thirdly, cell surface was stained for antibodies against CD45, CD127, and lineage on ice for 30 min. The fixing and permeabilizing of cells were performed using a transcription factor buffer set according to the product protocol. In the end, intracellular staining was performed with nuclear antibodies against RORγt. Cell sorting was performed by BD FACSVerse (BD Bioscience, New Jersey, USA), and flow cytometry data were analyzed with Flow Jo software V10 6.2 (BD Bioscience, New Jersey, USA).

Quantitative reverse transcription polymerase chain reaction analysis

Total intestinal RNA was obtained from mouse ileal tissue and extracted according to the commercial RNA extraction kit, and the total RNA was reverse-transcribed into cDNA using the HiScript III All-in-one RT SuperMix Perfect for qPCR; finally, the cDNA was mixed with primers and TB green premix Ex Taq II, and then amplified and quantized using Bioer qRT-PCR (Bioer, Hangzhou, China). The reaction conditions were as follows: 95 °C 30 s, 95 °C 5 s, and 60 °C 30 s. The primer was synthesized by Shenggong (Chengdu, China) with GAPDH as the internal reference gene. The qRT-PCR primers used in this study are shown in Table 1. The relative mRNA expression levels of the target gene were calculated using the 2$^{-\Delta\Delta Ct}$ method.

Histological and immunofluorescence analysis

2–3 cm ileum segments were fixed in 4% paraformaldehyde for at least 48 h, dehydrated and embedded in paraffin, cut into 4 μm slices, and then stained with hematoxylin–eosin (H&E) to observe the length of villi and the depth of crypts in

Table 1 Primer sequences

Primers	Sequence (5′ to 3′)
RORγt-F	GACCCACACCTCACAAATTGA
RORγt-R	AGTAGGCCACATTACACTGCT
IL-22-F	CTGAGAAATGCTTGCGTCTG
IL-22-R	CGTTAGCTTCTCACTTTCCTTTAG
IL-17A-F	TCCCTCTGTGATCTGGGAA
IL-17A-R	CTCGACCCTGAAAGTGAAGG
IL-10-F	CTTACTGACTGGCATGAGGATCA
IL-10-R	GCAGCTCTAGGAGCATGTGG
IL-22R-F	ATATTGTCCAAGGAAAGTGCCC
IL-22R-R	AGCCGACGAGGAAACCCAT
Occludin-F	CCCAGGCTTCTGGATCTATGT
Occludin-R	TCCATCTTTCTTCGGGGTTTTCA
ZO-1-F	CGCAGCCAGTTCAAACAAAGTTCC
ZO-1-R	GCAACATCAGCAATCGGTCCAAAG
NPC1L1-F	TGTTTGGTATGGAGAGTGTGGA
NPC1L1-R	GTCACAGCAGAGACTGACATTG
CD36-F	GTCTGTGCCATTAATCATGTCG
CD36-R	GTCTGTGCCATTAATCATGTCG

the tissue under a microscope (THUNDER DM6B, Leica, Wetzlar, Germany). For the further step of immunofluorescence staining, the paraffin-embedded slices were blocked in a blocking buffer (5% BSA in PBS) and incubated with primary antibodies against IL-22Rα1(1 : 100, MAB42941, R&D), RORγt (1 : 500, DF3196, Affinity), pSTAT3 (1 : 400, #9145T, Cell Signaling Technology), occludin (1 : 500, GB111401, Servicebio), and ZO-1 (1 : 500, GB111402, Servicebio) overnight at 4 °C. After cleaning, they were incubated with secondary antibodies at 37 °C for 50 min in the dark. After incubation, the slices were incubated with DAPI (G1012, Servicebio) in the dark at 37 °C for 10 min. Finally, the slices were observed under a microscope, and the average fluorescence intensity was analyzed by ImageJ 1.52a (Rawak Software Inc., Stuttgart, Germany).

Gut microbiota analysis

Firstly, total DNA from the fecal microbial samples of C57BL/6 mice was extracted by using CTAB according to the manufacturer's instructions. Secondly, the V3–V4 variable regions on bacterial 16S rDNA gene were amplified using a forward primer (341F 5′-CCTACGGGNGGCWGCAG-3′) and a reverse primer (805R 5′-GACTACHVGGGTATCTAATCC-3′). The PCR products were purified and quantified using AMPure XT beads (Beckman Coulter Genomics, Danvers, MA, USA) and Qubit (Invitrogen, USA), respectively. Then, the amplicon pools were assessed on an Agilent 2100 Bioanalyzer (Agilent, USA) and Illumina (Kapa Biosciences, Woburn, MA, USA). Finally, NovaSeq 6000 was used for 2×250 bp double-ended sequencing. Raw data were obtained by computer sequencing, while clean data were obtained after a series of processing. After dereplication using DADA2, the final ASV feature table and feature sequence were obtained for subsequent diversity analysis, species classification annotation, and difference analysis. Principal coordinate analysis (PCoA), principal component analysis (PCA), and Pearson correlation analysis were performed by R version 3.6.3, while GraphPad Prism 9.0 was used for Chao1, Shannon, and species abundance analysis.

Western blotting

RIPA lysis buffer was added to 50 mg of ileal tissue, after cracking on ice, centrifuging at 12 000g for 15 min, taking the supernatant, and determining the total protein concentration. The protein samples were transferred to a polyvinylidene fluoride (PVDF) membrane by SDS-PAGE electrophoresis and blocked with 5% (w/v) defatted milk at room temperature. PVDF membrane was incubated with primary antibody NPClL1(1 : 1000, sc-166802, Santa Cruz Biotechnology Inc.) and CD36(1 : 1000, ab252923, Abcam) overnight at 4 °C and then incubated with horseradish peroxidase-conjugated secondary antibody β-tubulin (1 : 3000, A01857-1, Boster) at room temperature for 1.5 h. Protein bands were detected with an ultra-high sensitivity ECL kit and taken with the ChemiDocTM imaging system (Bio-Rad, Hercules, CA, USA) and adjusted to the appropriate exposure contrast. ImageJ software was used to quantify the western blot results.

Statistical analysis

All data were expressed as the mean ± SEM. GraphPad Prism 9.0 (GraphPad Prism software, San Diego, California, USA) was used to perform the statistical analysis. Statistical differences were analyzed by Student's t-test or one-way analysis of variance (ANOVA) with Tukey's test. Kruskal–Wallis rank sum test was performed to show the significance of the difference in alpha diversity. Pearson correlation analysis was performed to show the relationship between two parameters. Differences between experimental groups were considered statistically significant at p values <0.05.

Results

Limonin improved HFD-induced dyslipidemia

To assess the protective effect of limonin against HFD-induced dyslipidemia, we conducted experiments using male C57BL/6 mice fed with an HFD or ND, with or without limonin supplementation. Subsequent evaluations revealed that limonin administration dramatically inhibited weight gain in HFD-fed mice (Fig. 1C), as evidenced by the relative weight gain rate (ESI Fig. 1A†). The trend of Lee's index was consistent with that of body weight (Fig. 1D). Additionally, the accumulation of epididymal white fat and liver weight gain were markedly reduced with limonin treatment compared to that in the HFD group (Fig. 1E and F). There was no significant change in food intake between different interventions (ESI Fig. 1B†). At the end of the experiment, while HFD prominently increased serum levels of TC and LDL-C, limonin supplementation significantly lowered them (Fig. 1G and H). Serum levels of HDL-C were markedly decreased in the HFD group, whereas they were distinctly improved in the HFD + Lim group (Fig. 1I). However, no significant changes were observed in serum TG levels between the HFD group and HFD + Lim group (Fig. 1J). Moreover, limonin administration mitigated liver function as indicated by the levels of ALT and AST in the HFD + Lim group relative to the HFD group (Fig. 1K and L).

Limonin eased the impaired intestinal barrier in HFD-fed mice

H&E staining revealed a markedly reduced villus height in HFD-fed mice (Fig. 2A). Rather, the pathological changes caused by HFD were ameliorated by the administration of limonin, which exhibited longer villi and greater crypt depth than HFD-fed mice (Fig. 2B and C). Immunofluorescence staining indicated that the levels of intestine tight junction proteins, occludin and Zonula occludens-1 (ZO-1) significantly decreased in the intestinal epithelium in HFD-fed mice (Fig. 2D–F and H). The impaired tight junction proteins were significantly alleviated after limonin treatment. In keeping with this, these findings were further confirmed by qRT-PCR analysis that limonin treatment increased the lowered mRNA levels of occludin and ZO-1 in HFD-fed mice (Fig. 2G and I).
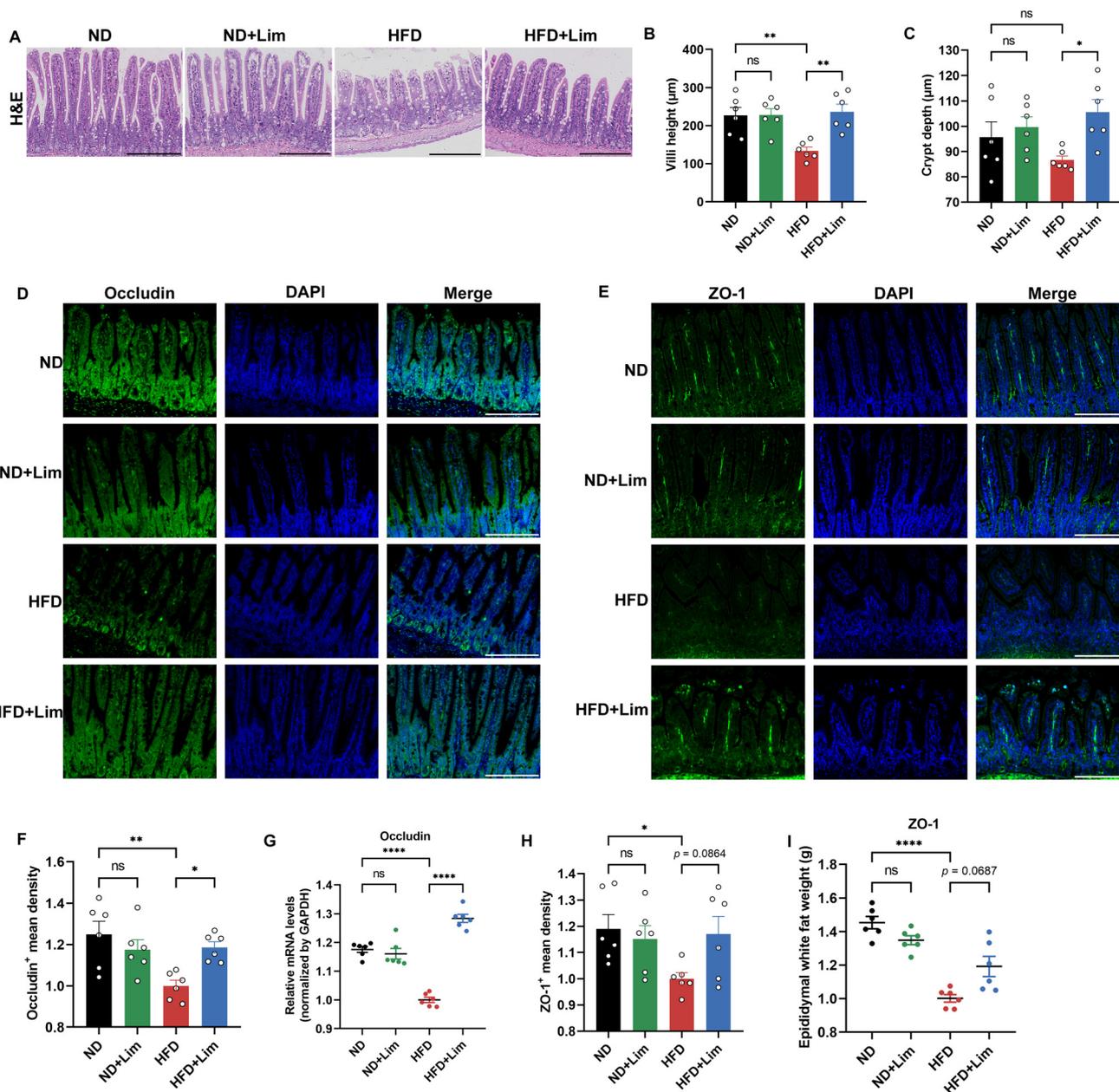
Fig. 2 Limonin eased impaired intestinal barrier in HFD-fed mice. (A) H&E staining was measured for (B) the villus height and (C) crypt height. Scale bars, 200 μm. (D and E) Representative immunofluorescence images of occludin⁺ cells and ZO-1⁺ cells in ileum tissues (original magnification ×400). Green: positive staining of occludin and ZO-1; blue: DAPI; scale bars, 200 μm. (F and H) Fluorescence intensity of occludin and ZO-1. (G and I) qRT-PCR analysis of occludin and ZO-1. All data were expressed as mean ± SEM with 6 samples in each group. *$p < 0.05$; ** $p < 0.01$; *** $p < 0.001$; **** $p < 0.0001$.

Limonin modulated the structural composition of the gut microbiota in HFD-fed mice

To explore the potential relationship of limonin to HFD-induced gut microbiota dysbiosis, we performed 16S rRNA gene sequencing after 16 weeks of dietary intervention. As we observed in the PCoA (beta diversity) analysis, the structure of the gut microbiota formed different clusters among the four groups (Fig. 3A). Specifically, the gut microbiota structure of the ND group and ND + Lim group almost overlapped, forming a significant difference from the HFD group, while the cluster of the HFD + Lim group was closer to the ND group and ND + Lim group. Similar results were also confirmed in the PCA analysis (ESI Fig. 2A†). Together, these results suggest that HFD altered the structural composition of the gut microbiota, while limonin supplementation effectively ameliorated HFD-induced gut microbiota dysbiosis. However, the Chao1 index and Shannon index (alpha diversity) revealed no signifi-
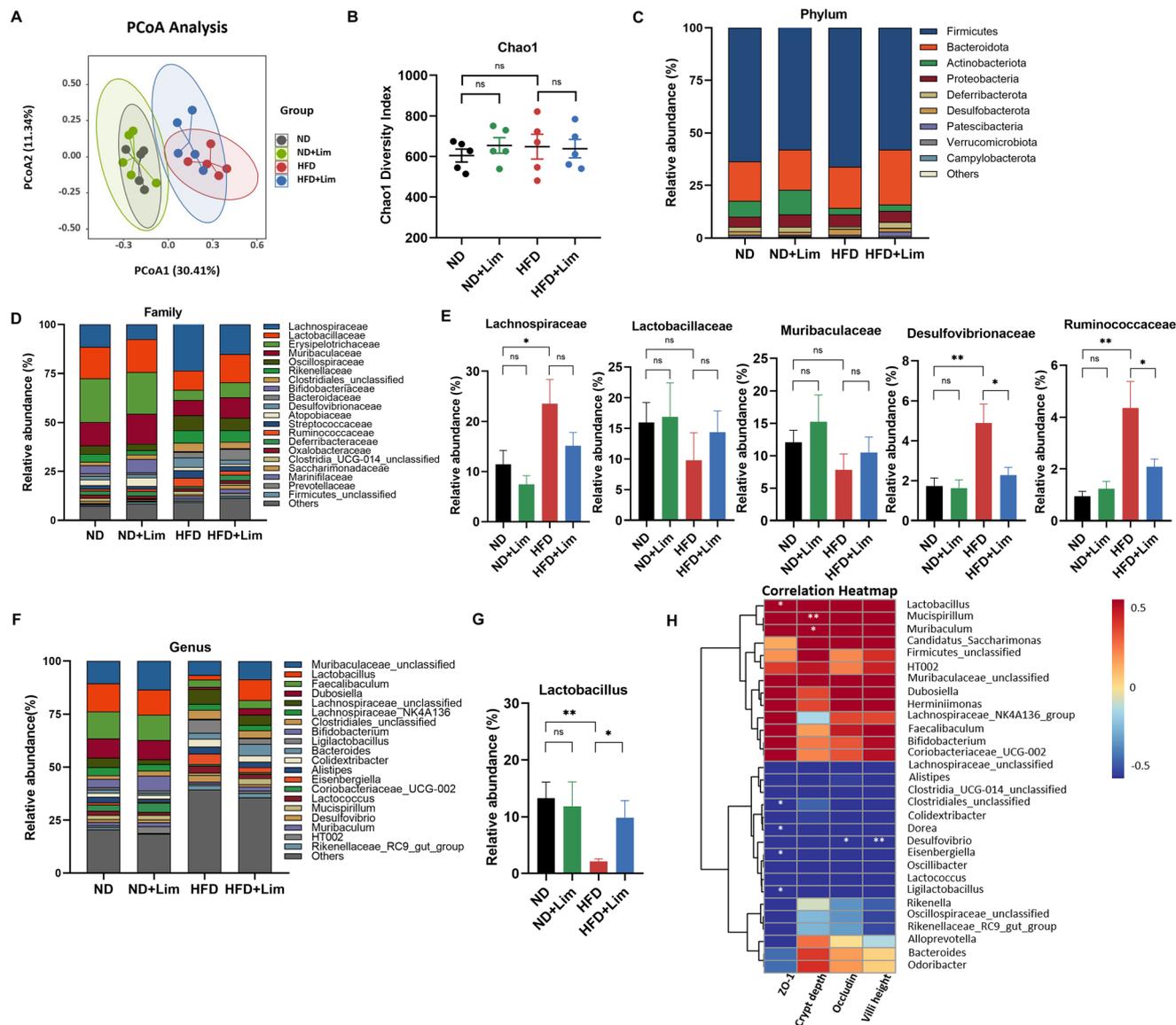
Fig. 3 Limonin modulated the structural composition of the gut microbiota in HFD-fed mice. (A) PCoA analysis (beta diversity) based on Bray–Curtis distance. (B) Chao1 diversity index (alpha diversity). The relative abundance of bacteria at (C) the phylum level. The relative abundance of bacteria at (D) the family level and (E) relative abundance of identified differential abundant bacterial groups at the family level. The relative abundance of bacteria at (F) the genus level and (G) *Lactobacillus*. All data were expressed as mean ± SEM with 5 samples in each group. *$p < 0.05$; ** $p < 0.01$; *** $p < 0.001$; **** $p < 0.0001$. (H) Pearson correlation analysis was performed between genus bacteria and indicators of the intestinal barrier. The color scales represent the strength of correlation, ranging from 0.5 (strong positive) to −0.5 (strong negative correlation).

cant difference among the four groups, indicating that different interventions did not result in significant changes in species richness between the four groups (Fig. 3B) (ESI Fig. 2B†). To further investigate the specific changes in the gut microbiota, we further analyzed the relative abundance of the phylum, family, and genus level. Firmicutes and Bacteroidota were the major components of the phylum level, accounting for 80% of the total abundance (Fig. 3C). HFD was associated with significant alterations in gut microbiota composition, including an increase in the relative abundance of Firmicutes, Desulfobacterota, and Campylobacterota and a decrease in

the relative abundance of Deferribacterota. Limonin reversed the HFD-induced changes in the gut microbiota. At the family level, limonin supplementation increased the abundance of *Lactobacillaceae* and *Muribaculaceae* while decreasing the abundance of *Lachnospiraceae*, *Desulfovibrionaceae*, and *Ruminococcaceae* in the HFD + Lim group compared to the HFD group (Fig. 3D and E). At the genus level, the proportion of probiotic *Muribaculaceae_unclassified*, *Lactobacillus*, *Dubosiella*, and *Muribaculum* was depleted; instead, the proportion of pathogenic *Lachnospiraceae_unclassified*, *Alistipes*, *Eisenbergiella*, *Desulfovibrio*, *Clostridia_UCG-*

014, and *Ruminococcaceae_unclassified* was increased in the HFD group compared with the ND group (Fig. 3F) (ESI Fig. 2C†). Limonin supplementation reversed the HFD-induced alteration in the gut microbiota to a certain extent, especially significantly increased the abundance of the probiotic *Lactobacillus* (Fig. 3G). Pearson correlation analysis showed the relationship between the HFD-induced gut microbiota and intestinal barrier. The analysis result revealed that *Clostridiales_unclassified*, *Dorea*, *Desulfovibrio*, and *Eisenbergiella* were negatively correlated with the intestinal barrier, while *Lactobacillus*, *Muribaculum*, and *Mucispirillum* were positively correlated with the intestinal barrier (Fig. 3H).

Limonin regulated the ILC3–IL22–IL22R pathway in HFD-fed mice to improve the impaired intestinal barrier

Emerging evidence has revealed that the ILC3–IL22–IL22R pathway plays a critical role in regulating the intestinal barrier function.[16–18]

In flow cytometry analysis, ILC3s were gated on $Lin^-CD45^+CD127^+ ROR\gamma t^+$ cells.[12] The proportion of $ROR\gamma t^+$ ILCs was higher in the HFD group relative to that in the ND group, while limonin significantly elevated the proportion of ILC3s in HFD-fed mice (Fig. 4A and B). In addition, in line with the flow cytometry results, the expression of $ROR\gamma t$ in
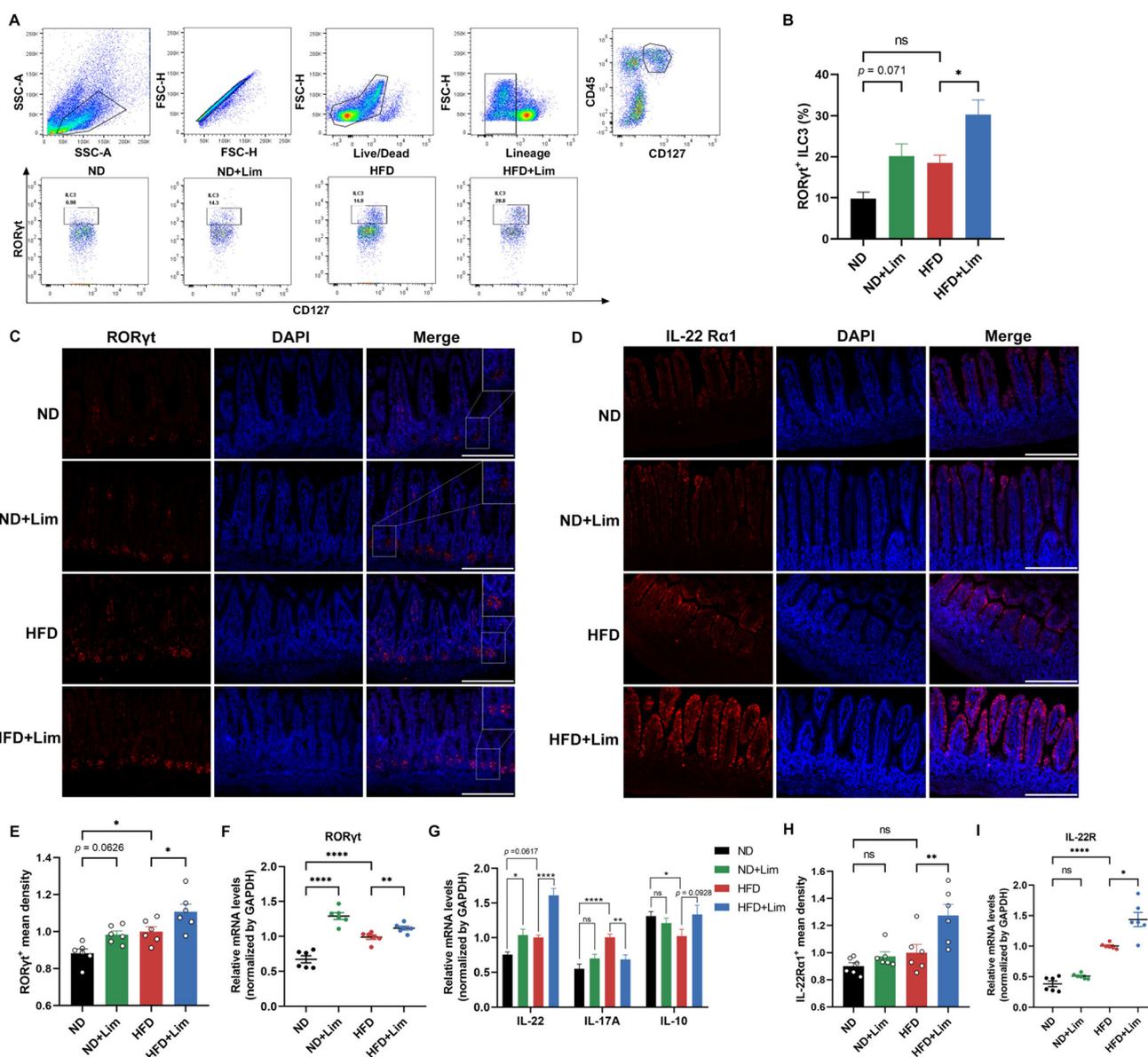

Fig. 4 Limonin regulated the ILC3–IL22–IL22R pathway in HFD-fed mice to improve impaired intestinal barrier. (A) Flow cytometry analysis of $Lin^-CD45^+CD127^+ROR\gamma t^+$ ILC3s; (B) the proportion of $ROR\gamma t^+$ ILC3; $n = 3$. (C and D) Representative immunofluorescence images of $ROR\gamma t^+$ cells and IL-22Rα1$^+$ cells in ileum tissues (original magnification ×400). Red: positive staining of $ROR\gamma t$ and IL-22Rα1; blue: DAPI; scale bars, 200 μm; $n = 6$. (E and H) Fluorescence intensity of $ROR\gamma t$ and IL-22Rα1. (F, G and I) qRT-PCR analysis of $ROR\gamma t$, IL-22, IL-17A, IL-10 and IL-22Rα1; $n = 6$. All data were expressed as mean ± SEM. $*p < 0.05$; $**p < 0.01$; $***p < 0.001$; $****p < 0.0001$.

both immunofluorescence and qRT-PCR was increased in the HFD + Lim group relative to that in the HFD group (Fig. 4C, E and F). Moreover, immunofluorescence staining demonstrated that ILC3s mainly resided in the lamina propria of the intestine. Then, we detected the mRNA expression of IL-22, IL-17A, and IL-10, which are closely related to ILC3s, and found that the expression of IL-22 and IL-17A was obviously increased in HFD-fed mice, while the expression of IL-10 was significantly decreased. Limonin supplementation markedly increased IL-22 levels in both ND and HFD-fed mice. In contrast, we found that IL-17A expression showed a sharp reduction in the HFD + Lim group. However, there is no significant difference in the IL-10 mRNA expression between the HFD + Lim group and the HFD group (Fig. 4G). The distribution of positive IL-22R staining was localized predominantly on the intestinal epithelial cell membrane (Fig. 4D). We found that the mean fluorescence intensity of IL-22R was significantly increased in the HFD + Lim group relative to the HFD group (Fig. 4H). Correspondingly, we observed higher mRNA expression of IL-22R in the HFD group, and the administration of limonin resulted in a dramatic upregulation of IL-22R mRNA levels in the HFD + Lim group (Fig. 4I).

Limonin improved lipid metabolism in IEC-activated mice

The transcription factor STAT3 is a key downstream signal of IL-22R.[32] In the present study, we observed that limonin treatment stimulated IECs with increased pSTAT3-positive cells in immunofluorescence staining in the HFD + Lim group compared with the HFD group (Fig. 5A and B). To further clarify whether the function of IECs restored by the ILC3–IL22–IL22R pathway has a positive effect on lipid metabolites, we confirmed the reduction of protein levels of key lipid transporters, including CD36 and Niemann–Pick C1-like 1 (NPC1L1) in the HFD + Lim group relative to the HFD group (Fig. 5D and E). Similar results were further confirmed at the mRNA levels (Fig. 5C). This change was associated with dramatically decreased lipid profiles and diminished epididymal fat accumulation and liver weight gain. Collectively, these results suggested that limonin upregulated the ILC3–IL22–IL22R pathway, and then activated pSTAT3 in IECs, thereby modulating key lipid transporters to ameliorate HFD-induced dyslipidemia.

Discussion

Our experiments revealed that limonin treatment significantly improved HFD-induced dyslipidemia by reducing serum TC and LDL-C levels and increasing the HDL-C levels in HFD-fed mice. Importantly, starting from the fourth week until the end of the experiment, limonin administration significantly reduced weight gain in the HFD + Lim group compared to the HFD group, demonstrating its significant preventive effect against HFD-induced weight gain. Limonin supplementation markedly reduced the accumulation of epididymal fat and liver weight gain induced by HFD. Moreover, the levels of ALT

and AST were significantly decreased in the HFD + Lim group compared to the HFD group. Collectively, these results suggest that limonin improved HFD-induced dyslipidemia and weight gain, as well as protected against HFD-induced hepatic injury.

Consistent with previous experiments, we noted that HFD caused damage to the intestinal barrier. H&E staining revealed an obvious reduction in villus length and crypt depth in the ileal tissue of HFD-fed mice. Using immunofluorescence and qRT-PCR, we confirmed that HFD markedly diminished the expression of tight junction proteins, including occludin and ZO-1. This alteration in tight junctions resulted in weakened barrier function and epithelial integrity.[33,34] Limonin supplementation dramatically increased crypt depth and villus length, as well as the expression of tight junction proteins in the HFD + Lim group, indicating a protective effect of limonin against HFD-induced damage to intestinal barrier.

Previous studies have demonstrated that eliminating HFD-induced microbiota with antibiotics can reverse HFD-induced intestinal barrier damage,[20,35] suggesting that HFD-induced intestinal barrier damage is associated with the gut microbiota. In our study, beta diversity analysis indicated that HFD altered the structure of the gut microbiota, but limonin supplementation can effectively mitigate this change. At the phylum level, HFD-induced intestinal microbiota dysbiosis in mice was characterized by an increased abundance of Firmicutes. The increased abundance of the family *Lachnospiraceae* in HFD-fed mice was involved in the development of obesity and diabetes.[36] *Ruminococcaceae* has been reported to be enriched in HFD-fed mice and the db/db mice, and to be involved in host lipid metabolism.[37] In addition, limonin supplementation reduced the family *Desulfovibrionaceae* and genus *Desulfovibrio*, a bacterium that produces LPS, to reduce inflammation and alleviate barrier function impairment.[8] At the genus level, the abundance of pathogenic *Alistipes*, *Eisenbergiella*, *Desulfovibrio*, *Clostridia_UCG-014*, and *Ruminococcaceae_unclassified* were found to be highly abundant in HFD-fed mice and contribute to impaired intestinal barrier function,[7,35,37,38] as supported by correlation analyses and other studies. Limonin treatment was sufficient to both reduce the abundance of HFD-enriched pathogenic bacteria and increase the abundance of probiotics, including *Muribaculaceae_unclassified*, *Lactobacillus*, *Dubosiella*, and *Muribaculum*. Pearson correlation analysis revealed a positive association between these probiotics and the integrity of intestinal barrier. Specifically, limonin-increased probiotics have been demonstrated to enhance the intestinal barrier function by producing SCFAs.[39–41] Notably, limonin supplementation significantly increased the abundance of *Lactobacillus* in the HFD + Lim group compared to the HFD group. *Lactobacillus* is known to stimulate the production of aryl hydrocarbon receptor (AHR) ligands that activate ILC3s to stimulate the expression of the crucial barrier factor IL-22, thereby improving metabolic function and strengthening intestinal barrier integrity.[42] Taken together, we concluded that the potential mechanism of limonin supplementation to alleviate HFD-induced intestinal barrier damage and dyslipidemia may
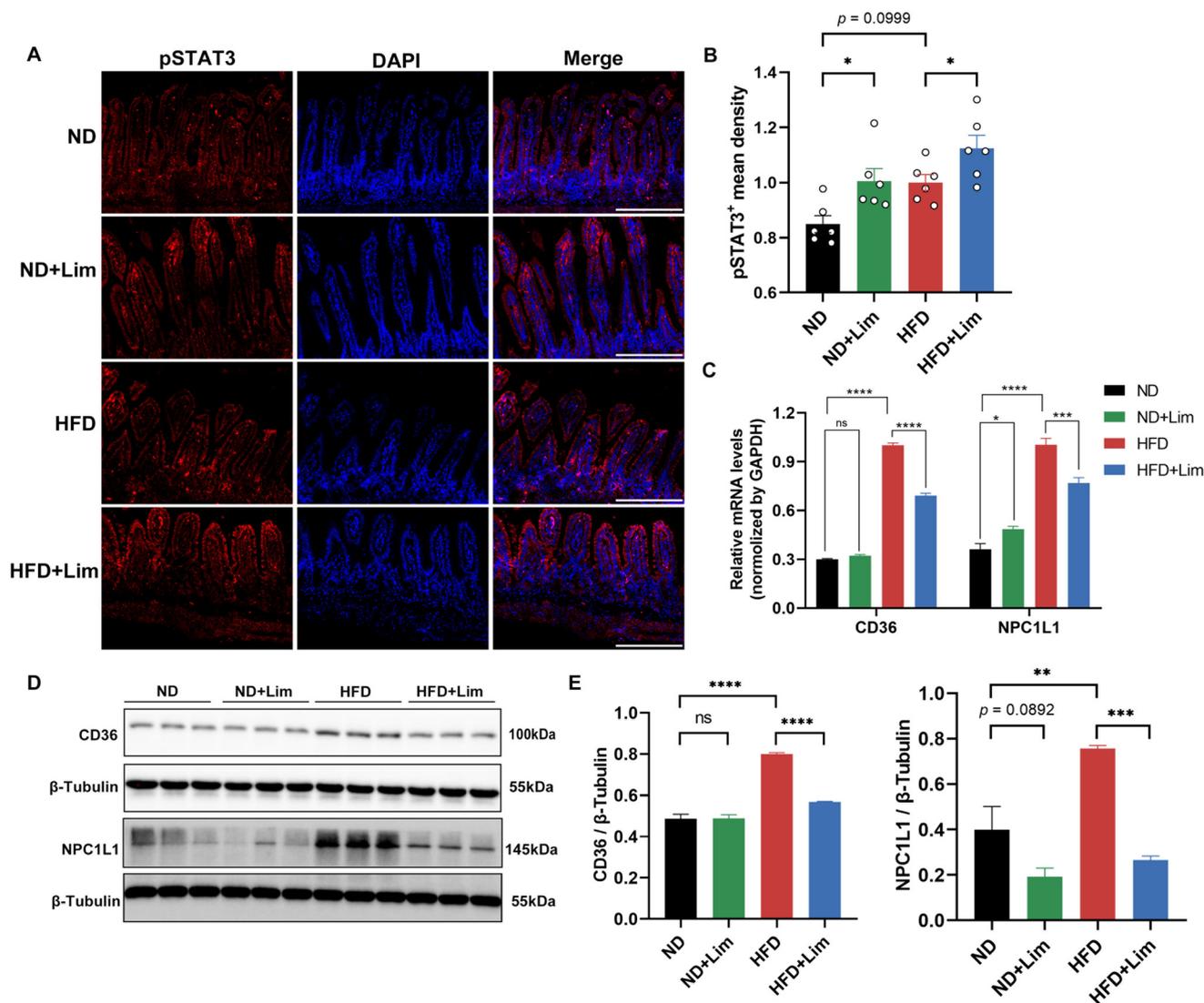
Fig. 5 Limonin improved lipid metabolism in IEC-activated mice. (A) Representative immunofluorescence images of pSTAT3 cells in ileum tissues (original magnification ×400). Red: positive staining of pSTAT3; blue: DAPI; scale bars, 200 μm; $n = 6$. (B) Fluorescence intensity of pSTAT3. (C) qRT–PCR analysis of intestinal key lipid transporters CD36 and NPC1L1, $n = 6$. (D and E) The protein levels of intestinal key lipid transporters CD36 and NPC1L1, $n = 3$. All data were expressed as mean ± SEM. *$p < 0.05$; ** $p < 0.01$; *** $p < 0.001$; **** $p < 0.0001$.

be achieved through microbiota-induced ILC3–IL22–IL22R pathway.

In our investigation, flow cytometry and other analyses revealed that HFD increased the proportion of intestinal ILC3s. Previous studies have reported that exposure to HFD by mothers and their offspring resulted in a unique microbiota characterized by an increase in Firmicutes, and the expansion of ILC3s.[43] Specifically, the mono-colonization of segmented filamentous bacteria (SFB), a type of Firmicutes, in germ-free Rag1$^{-/-}$ mice led to the activation of ILC3s.[19,44] Furthermore, it has been shown that HFD also increased ILC3s in the liver, which stimulated the production of IL-22 to alleviate liver fibrosis and hepatic steatosis.[45] Interestingly, our study found that the administration of limonin significantly upregulated the expression of ILC3s in HFD-fed mice, more so than in the

HFD group alone. To further explore the mechanism of ILC3s under HFD intervention and limonin supplementation, we investigated the mRNA levels of cytokines IL-22, IL-17A, and IL-10. We confirmed that HFD-enriched ILC3s promoted an obvious increase in both IL-22 and IL-17A mRNA levels. However, limonin-activated ILC3s significantly increased IL-22 mRNA levels and simultaneously decreased IL-17A mRNA levels. IL-17A can stimulate a variety of cells, including epithelial cells, to activate pro-inflammatory cytokines.[46] Although it has been reported that inappropriate activation of ILC3s in inflammatory bowel disease results in distinctly higher expression of IL-22 than in healthy individuals,[47] IL-22 has also been reported to play an integral role in promoting the recovery of colitis models, including colonic thickness disease score, body mass index, and mortality.[48,49] Intestinal

IL-22 production is strictly restricted to NCR$^+$ ILC3s, a subset of ILC3s that account for 70% of the entire intestinal ILCs, whereas IL-17A is predominantly produced by NCR$^-$ ILC3s, which accounts for only 15%.[50,51] In the presence of IL-1β plus IL-23, the increased NCR$^-$ ILC3s can be transformed into NCR$^+$ ILC3s.[52] Therefore, we speculated that HFD-increased NCR$^-$ ILC3s significantly upregulated IL-17A mRNA, which leads to a series of pro-inflammatory activities. At the same time, under the stimulation of certain cytokines, increased NCR$^-$ ILC3s can be converted into NCR$^+$ ILC3s, thereby increasing the anti-inflammatory effect of IL-22, which may be compensation for the significant elevation of IL-17A. In brief, HFD-enriched ILC3s play a double-edged role as both anti-inflammatory and pro-inflammatory factors in the intestinal barrier. Notably, limonin intervention significantly upregulated IL-22, but not IL-17A, suggesting that limonin primarily promotes the production of IL-22-producing NCR$^+$ ILC3s, thus playing a protective role in lipid metabolism and intestinal barrier. In addition, HFD significantly reduced IL-10 mRNA levels, while limonin intervention could partially increase them. ILCreg-derived IL-10 can noticeably inhibit the production of IL-17A by NCR$^-$ ILC3s, reducing the pro-inflammatory activation.[52] Therefore, we can conclude that the mechanism of activation of ILC3s is different under HFD intervention and limonin intervention.

Strikingly, IL-22 is not only a critical barrier factor but also has the potential to regulate metabolism. Studies have found that HFD-fed mice deficient in IL-22 receptors are prone to developing metabolic disorders, and supplementation of exogenous IL-22 can regulate lipid metabolism in HFD-fed mice with significantly reduced body weight and epididymal fat-pad mass.[53] In addition, IL-22RA1-deficient mice displayed higher weight gain after HFD intervention and subsequently developed higher levels of insulin resistance and glucose intolerance within 3 months, which was significantly reversed after intervention with exogenous IL-22.[53] IL-22 produced by ILC3s has recently been shown to regulate lipid metabolism by regulating key lipid transporters, including CD36, NPC1L1, Fabp1, and Fabp2.[19] Meanwhile, other studies have also demonstrated that the inhibition of ILC3s to reduce IL-22 secretion leads to a decrease in the epithelial cell-derived antimicrobial peptides (*e.g.* RegIIIγ) and an increase in lipid transporters (*e.g.* Fabp2, CD36).[54] Thus, the ILC3–IL22–IL22R pathway regulates lipid metabolism at least in part by controlling lipid transporters. To further explore the relationship between the ILC3–IL22–IL22R pathway and lipid transporters, we examined IL-22R expressed in IECs and the downstream key transcription factor STAT3. In our study, limonin supplementation markedly promoted the expression of IL-22RA1 and pSTAT3 in the IECs. This activation leads to the protection of the intestinal barrier by inducing the production of antimicrobial peptides in epithelial cells. We further examined the levels of specific lipid transporters CD36 and NPC1L1 expressed in the intestine. Limonin supplementation significantly reduced the protein levels and mRNA expression of key intestinal lipid transporters CD36 and NPC1L1 in the HFD + Lim group compared to the
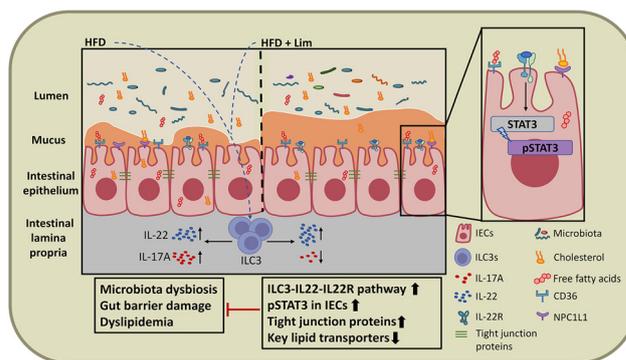

Fig. 6 Schematic summary of the ILC3−IL22−IL22R pathway in the gut under different interventions of HFD and HFD supplemented with limonin.

HFD group. This suggests that limonin intervention regulated the ILC3–IL22–IL22R pathway, and promoted the phosphorylation of STAT3 in IECs to restore the intestinal barrier function, ultimately leading to the reduction of key lipid transporters to ameliorate HFD-induced dyslipidemia.

Conclusions

In summary, our results confirmed that limonin improved HFD-induced dyslipidemia and weight gain, and reduced epididymal white fat weight while preventing HFD-induced hepatic injury. HFD-increased Firmicutes partly activated ILC3s and then promoted the production of IL-17A and IL-22, playing a complex role in the intestinal barrier. Limonin supplementation distinctly enriched *Lactobacillus* in HFD-fed mice, predominantly activated ILC3s to produce IL-22, promoted pSTAT3 in IECs, enhanced tight junction protein, and increased villus length and crypt depth. Finally, we determined that limonin treatment significantly reduced the mRNA and protein levels of intestinal lipid transporters CD36 and NPC1L1 in the HFD + Lim group. Taken together, these results suggest that limonin administration significantly upregulated the microbiota-mediated ILC3–IL22–IL22R pathway to restore HFD-induced intestinal barrier damage, resulting in the reduction of key lipid transporters and ultimately ameliorating HFD-induced dyslipidemia (Fig. 6). However, the research on ILC3 is still in the nascent stage. The synergistic effect of ILC3 with other immune cells and cytokines involves more complex mechanisms, which may further explain the double-edged sword role of ILC3s in regulating the intestinal barrier. We will continue to follow up on relevant studies in the future.

Author contributions

W. L. W. performed the research, carried out the data collection and analysis, and drafted the manuscript. Y. Y. P. assisted with the assessment of lipid profile levels and participated in

the animal experiment part. H. Y. S. conducted the flow cytometry assays and analyses. T. Y. Z., X. L., and H. Y. Z. helped revise the manuscript. X. Z. provided experimental concepts and design, offered scientific direction, and guide the revision of the manuscript.

Conflicts of interest

There are no conflicts to declare.

Acknowledgements

References

1 M. Arvanitis and C. J. Lowenstein, Dyslipidemia, *Ann. Intern. Med.*, 2023, **176**, ITC81–ITC96.

2 A. Pirillo, M. Casula, E. Olmastroni, G. D. Norata and A. L. Catapano, Global epidemiology of dyslipidaemias, *Nat. Rev. Cardiol.*, 2021, **18**, 689–700.

3 A. Cieza, K. Causey, K. Kamenov, S. W. Hanson, S. Chatterji and T. Vos, Global estimates of the need for rehabilitation based on the Global Burden of Disease study 2019: a systematic analysis for the Global Burden of Disease Study 2019, *Lancet*, 2020, **396**, 2006–2017.

4 J. D. Stanaway, A. Afshin, E. Gakidou, S. S. Lim, D. Abate, K. H. Abate, C. Abbafati, *et al.*, Global, regional, and national comparative risk assessment of 84 behavioural, environmental and occupational, and metabolic risks or clusters of risks for 195 countries and territories, 1990–2017: a systematic analysis for the Global Burden of Disease Study 2017, *Lancet*, 2018, **392**, 1923–1994.

5 F. Vancheri, L. Backlund, L.-E. Strender, B. Godman and B. Wettermark, Time trends in statin utilisation and coronary mortality in Western European countries, *BMJ Open*, 2016, **6**, e010500.

6 C. K. Chow, T. N. Nguyen, S. Marschner, R. Diaz, O. Rahman, A. Avezum, S. A. Lear, K. Teo, K. E. Yeates, F. Lanas, W. Li, B. Hu, P. Lopez-Jaramillo, R. Gupta, R. Kumar, P. K. Mony, A. Bahonar, K. Yusoff, R. Khatib, K. Kazmi, A. L. Dans, K. Zatonska, K. F. Alhabib, I. M. Kruger, A. Rosengren, S. Gulec, A. Yusufali, J. Chifamba, S. Rangarajan, M. McKee and S. Yusuf, Availability and affordability of medicines and cardiovascular outcomes in 21 high-income, middle-income and low-income countries, *BMJ Global Health*, 2020, **5**, e002640.

7 X.-Y. Zhang, J. Chen, K. Yi, L. Peng, J. Xie, X. Gou, T. Peng and L. Tang, Phlorizin ameliorates obesity-associated endotoxemia and insulin resistance in high-fat diet-fed mice by targeting the gut microbiota and intestinal barrier integrity, *Gut Microbes*, 2020, **12**, 1–18.

8 Y. Wang, W. Yao, B. Li, S. Qian, B. Wei, S. Gong, J. Wang, M. Liu and M. Wei, Nuciferine modulates the gut microbiota and prevents obesity in high-fat diet-fed rats, *Exp. Mol. Med.*, 2020, **52**, 1959–1975.

9 B. Allam-Ndoul, S. Castonguay-Paradis and A. Veilleux, Gut Microbiota and Intestinal Trans-Epithelial Permeability, *Int. J. Mol. Sci.*, 2020, **21**, 6402.

10 C.-W. Ko, J. Qu, D. D. Black and P. Tso, Regulation of intestinal lipid metabolism: current concepts and relevance to disease, *Nat. Rev. Gastroenterol. Hepatol.*, 2020, **17**, 169–183.

11 X. Guo, J. Qiu, T. Tu, X. Yang, L. Deng, R. A. Anders, L. Zhou and Y.-X. Fu, Induction of Innate Lymphoid Cell-Derived Interleukin-22 by the Transcription Factor STAT3 Mediates Protection against Intestinal Infection, *Immunity*, 2014, **40**, 25–39.

12 M. Gury-BenAri, C. A. Thaiss, N. Serafini, D. R. Winter, A. Giladi, D. Lara-Astiaso, M. Levy, T. M. Salame, A. Weiner, E. David, H. Shapiro, M. Dori-Bachash, M. Pevsner-Fischer, E. Lorenzo-Vivas, H. Keren-Shaul, F. Paul, A. Harmelin, G. Eberl, S. Itzkovitz, A. Tanay, J. P. Di Santo, E. Elinav and I. Amit, The Spectrum and Regulatory Landscape of Intestinal Innate Lymphoid Cells Are Shaped by the Microbiome, *Cell*, 2016, **166**, 1231–1246.

13 S. Cording, J. Medvedovic, M. Cherrier and G. Eberl, Development and regulation of RORγt+ innate lymphoid cells, *FEBS Lett.*, 2014, **588**, 4176–4181.

14 K.-A. G. Buela, S. Omenetti and T. T. Pizarro, Cross-talk between type 3 innate lymphoid cells and the gut microbiota in inflammatory bowel disease, *Curr. Opin. Gastroenterol.*, 2015, **31**, 449–455.

15 R. Campana, S. Federici, E. Ciandrini and W. Baffone, Antagonistic Activity of Lactobacillus acidophilus ATCC 4356 on the Growth and Adhesion/Invasion Characteristics of Human Campylobacter jejuni, *Curr. Microbiol.*, 2012, **64**, 371–378.

16 M. A. Kinnebrew, C. Ubeda, L. A. Zenewicz, N. Smith, R. A. Flavell and E. G. Pamer, Bacterial Flagellin Stimulates Toll–Like Receptor 5-Dependent Defense against Vancomycin–ResistantEnterococcusInfection, *J. Infect. Dis.*, 2010, **201**, 534–543.

17 M. A. Kinnebrew, C. G. Buffie, G. E. Diehl, L. A. Zenewicz, I. Leiner, T. M. Hohl, R. A. Flavell, D. R. Littman and E. G. Pamer, Interleukin 23 Production by Intestinal CD103+CD11b+ Dendritic Cells in Response to Bacterial Flagellin Enhances Mucosal Innate Immune Defense, *Immunity*, 2012, **36**, 276–287.

18 C. A. Lindemans, M. Calafiore, A. M. Mertelsmann, M. H. O'Connor, J. A. Dudakov, R. R. Jenq, E. Velardi, L. F. Young, O. M. Smith, G. Lawrence, J. A. Ivanov, Y.-Y. Fu, S. Takashima, G. Hua, M. L. Martin, K. P. O'Rourke, Y.-H. Lo, M. Mokry, M. Romera-Hernandez, T. Cupedo, L. E. Dow, E. E. Nieuwenhuis, N. F. Shroyer, C. Liu, R. Kolesnick, M. R. M. van den Brink and A. M. Hanash, Interleukin-22 promotes intestinal-stem-cell-

mediated epithelial regeneration, *Nature*, 2015, **528**, 560–564.

19 K. Mao, A. P. Baptista, S. Tamoutounour, L. Zhuang, N. Bouladoux, A. J. Martins, Y. Huang, M. Y. Gerner, Y. Belkaid and R. N. Germain, Innate and adaptive lymphocytes sequentially shape the gut microbiota and lipid metabolism, *Nature*, 2018, **554**, 255–259.

20 J. Zou, B. Chassaing, V. Singh, M. Pellizzon, M. Ricci, M. D. Fythe, M. V. Kumar and A. T. Gewirtz, Fiber-Mediated Nourishment of Gut Microbiota Protects against Diet-Induced Obesity by Restoring IL-22-Mediated Colonic Health, *Cell Host Microbe*, 2018, **23**, 41–53.

21 F. Bäckhed, J. K. Manchester, C. F. Semenkovich and J. I. Gordon, Mechanisms underlying the resistance to diet-induced obesity in germ-free mice, *Proc. Natl. Acad. Sci. U. S. A.*, 2007, **104**, 979–984.

22 V. K. Ridaura, J. J. Faith, F. E. Rey, J. Cheng, A. E. Duncan, A. L. Kau, N. W. Griffin, V. Lombard, B. Henrissat, J. R. Bain, M. J. Muehlbauer, O. Ilkayeva, C. F. Semenkovich, K. Funai, D. K. Hayashi, B. J. Lyle, M. C. Martini, L. K. Ursell, J. C. Clemente, W. Van Treuren, W. A. Walters, R. Knight, C. B. Newgard, A. C. Heath and J. I. Gordon, Gut Microbiota from Twins Discordant for Obesity Modulate Metabolism in Mice, *Science*, 2013, **341**, 1241214.

23 K. E. Bouter, D. H. van Raalte, A. K. Groen and M. Nieuwdorp, Role of the Gut Microbiome in the Pathogenesis of Obesity and Obesity-Related Metabolic Dysfunction, *Gastroenterology*, 2017, **152**, 1671–1678.

24 S. M. Jandhyala, R. Talukdar, C. Subramanyam, H. Vuyyuru, M. Sasikala and D. Nageshwar Reddy, Role of the normal gut microbiota, *World J. Gastroenterol.*, 2015, **21**, 8787–8803.

25 H. Wu, S. Xie, J. Miao, Y. Li, Z. Wang, M. Wang and Q. Yu, Lactobacillus reuteri maintains intestinal epithelial regeneration and repairs damaged intestinal mucosa, *Gut Microbes*, 2020, **11**, 997–1014.

26 J. Cheng, A. Laitila and A. C. Ouwehand, Bifidobacterium animalis subsp. lactis HN019 Effects on Gut Health: A Review, *Front. Nutr.*, 2021, **8**, 790561.

27 S. Fan, C. Zhang, T. Luo, J. Wang, Y. Tang, Z. Chen and L. Yu, Limonin: A Review of Its Pharmacology, Toxicity, and Pharmacokinetics, *Molecules*, 2019, **24**, 3679.

28 M. Gu, J. Sun, C. Qi, X. Cai, T. Goulette, M. Song, X. You, D. A. Sela and H. Xiao, The gastrointestinal fate of limonin and its effect on gut microbiota in mice, *Food Funct.*, 2019, **10**, 5521–5530.

29 B. Jia, L. Zhao, P. Liu, M. Li and Z. Tian, Limonin ameliorates indomethacin–induced intestinal damage and ulcers through Nrf2/ARE pathway, *Immun., Inflammation Dis.*, 2023, **11**, e787.

30 D. Halder, N. D. Das, K. H. Jung, M. R. Choi, M. S. Kim, S. R. Lee and Y. G. Chai, Cyclodextrin-Clathrated Limonin Suppresses Diet-Induced Obesity in Mice, *J. Food Biochem.*, 2014, **38**, 216–226.

31 Y. Li, M. Yang, H. Lin, W. Yan, G. Deng, H. Ye, H. Shi, C. Wu, G. Ma, S. Xu, Q. Tan, Z. Gao and L. Gao, Limonin Alleviates Non-alcoholic Fatty Liver Disease by Reducing Lipid Accumulation, Suppressing Inflammation and Oxidative Stress, *Front. Pharmacol.*, 2022, **12**, 801730.

32 H.-X. Wei, B. Wang and B. Li, IL-10 and IL-22 in Mucosal Immunity: Driving Protection and Pathology, *Front. Immunol.*, 2020, **11**, 1315.

33 G. P. Ramos and K. A. Papadakis, Mechanisms of Disease: Inflammatory Bowel Diseases, *Mayo Clin. Proc.*, 2019, **94**, 155–165.

34 C. T. Capaldo, D. N. Powell and D. Kalman, Layered defense: how mucus and tight junctions seal the intestinal barrier, *J. Mol. Med.*, 2017, **95**, 927–934.

35 J. Yang, H. Wei, Y. Zhou, C.-H. Szeto, C. Li, Y. Lin, O. O. Coker, H. C. H. Lau, A. W. H. Chan, J. J. Y. Sung and J. Yu, High-Fat Diet Promotes Colorectal Tumorigenesis Through Modulating Gut Microbiota and Metabolites, *Gastroenterology*, 2022, **162**, 135–149.

36 B. Tian, Y. Geng, P. Wang, M. Cai, J. Neng, J. Hu, D. Xia, W. Cao, K. Yang and P. Sun, Ferulic acid improves intestinal barrier function through altering gut microbiota composition in high-fat diet-induced mice, *Eur. J. Nutr.*, 2022, **61**, 3767–3783.

37 M. Chamaillard, K.-A. Kim, W. Gu, I.-A. Lee, E.-H. Joh and D.-H. Kim, High Fat Diet-Induced Gut Microbiota Exacerbates Inflammation and Obesity in Mice via the TLR4 Signaling Pathway, *PLoS One*, 2012, **7**, e47713.

38 Z. Saqib, G. De Palma, J. Lu, M. Surette, P. Bercik and S. M. Collins, Alterations in fecal β-defensin-3 secretion as a marker of instability of the gut microbiota, *Gut Microbes*, 2023, **15**, 2233679.

39 L. Zheng, C. J. Kelly, K. D. Battista, R. Schaefer, J. M. Lanis, E. E. Alexeev, R. X. Wang, J. C. Onyiah, D. J. Kominsky and S. P. Colgan, Microbial-Derived Butyrate Promotes Epithelial Barrier Function through IL-10 Receptor–Dependent Repression of Claudin-2, *J. Immunol.*, 2017, **199**, 2976–2984.

40 H. Zhang, J. Xu, Q. Wu, H. Fang, X. Shao, X. Ouyang, Z. He, Y. Deng and C. Chen, Gut Microbiota Mediates the Susceptibility of Mice to Sepsis-Associated Encephalopathy by Butyric Acid, *J. Inflammation Res.*, 2022, **15**, 2103–2119.

41 J. Huang, D. Liu, Y. Wang, L. Liu, J. Li, J. Yuan, Z. Jiang, Z. Jiang, W. L. W. Hsiao, H. Liu, I. Khan, Y. Xie, J. Wu, Y. Xie, Y. Zhang, Y. Fu, J. Liao, W. Wang, H. Lai, A. Shi, J. Cai, L. Luo, R. Li, X. Yao, X. Fan, Q. Wu, Z. Liu, P. Yan, J. Lu, M. Yang, L. Wang, Y. Cao, H. Wei and E. L.-H. Leung, Ginseng polysaccharides alter the gut microbiota and kynurenine/tryptophan ratio, potentiating the antitumour effect of antiprogrammed cell death 1/programmed cell death ligand 1 (anti-PD-1/PD-L1) immunotherapy, *Gut*, 2022, **71**, 734–745.

42 W. M. de Vos, H. Tilg, M. Van Hul and P. D. Cani, Gut microbiome and health: mechanistic insights, *Gut*, 2022, **71**, 1020–1032.

43 S. T. Babu, X. Niu, M. Raetz, R. C. Savani, L. V. Hooper and J. Mirpuri, Maternal high-fat diet results in microbiota-

dependent expansion of ILC3s in mice offspring, *JCI Insight*, 2018, **3**, e99223.

44 T. Sano, W. Huang, J. A. Hall, Y. Yang, A. Chen, S. J. Gavzy, J.-Y. Lee, J. W. Ziel, E. R. Miraldi, A. I. Domingos, R. Bonneau and D. R. Littman, An IL-23R/IL-22 Circuit Regulates Epithelial Serum Amyloid A to Promote Local Effector Th17 Responses, *Cell*, 2015, **163**, 381–393.

45 M. Hamaguchi, T. Okamura, T. Fukuda, K. Nishida, Y. Yoshimura, Y. Hashimoto, E. Ushigome, N. Nakanishi, S. Majima, M. Asano, M. Yamazaki, H. Takakuwa, M. Kita and M. Fukui, Group 3 Innate Lymphoid Cells Protect Steatohepatitis From High-Fat Diet Induced Toxicity, *Front. Immunol.*, 2021, **12**, 648754.

46 R. Muir, M. Osbourn, A. V. Dubois, E. Doran, D. M. Small, A. Monahan, C. M. O'Kane, K. McAllister, D. C. Fitzgerald, A. Kissenpfennig, D. F. McAuley and R. J. Ingram, Innate Lymphoid Cells Are the Predominant Source of IL-17A during the Early Pathogenesis of Acute Respiratory Distress Syndrome, *Am. J. Respir. Crit. Care Med.*, 2016, **193**, 407–416.

47 R. S. Longman, G. E. Diehl, D. A. Victorio, J. R. Huh, C. Galan, E. R. Miraldi, A. Swaminath, R. Bonneau, E. J. Scherl and D. R. Littman, CX3CR1+ mononuclear phagocytes support colitis-associated innate lymphoid cell production of IL-22, *J. Exp. Med.*, 2014, **211**, 1571–1583.

48 K. Sugimoto, A. Ogawa, E. Mizoguchi, Y. Shimomura, A. Andoh, A. K. Bhan, R. S. Blumberg, R. J. Xavier and A. Mizoguchi, IL-22 ameliorates intestinal inflammation in a mouse model of ulcerative colitis, *J. Clin. Invest.*, 2008, **118**, 534–544.

49 C. Neufert, G. Pickert, Y. Zheng, N. Wittkopf, M. Warntjen, A. Nikolae, W. Ouyang, M. F. Neurath and C. Becker, Activation of epithelial STAT3 regulates intestinal homeostasis, *Cell Cycle*, 2014, **9**, 652–655.

50 J. H. Bernink, L. Krabbendam, K. Germar, E. de Jong, K. Gronke, M. Kofoed-Nielsen, J. M. Munneke, M. D. Hazenberg, J. Villaudy, C. J. Buskens, W. A. Bemelman, A. Diefenbach, B. Blom and H. Spits, Interleukin-12 and -23 Control Plasticity of CD127+ Group 1 and Group 3 Innate Lymphoid Cells in the Intestinal Lamina Propria, *Immunity*, 2015, **43**, 146–160.

51 L. A. Monticelli, G. F. Sonnenberg, M. C. Abt, T. Alenghat, C. G. K. Ziegler, T. A. Doering, J. M. Angelosanto, B. J. Laidlaw, C. Y. Yang, T. Sathaliyawala, M. Kubota, D. Turner, J. M. Diamond, A. W. Goldrath, D. L. Farber, R. G. Collman, E. J. Wherry and D. Artis, Innate lymphoid cells promote lung-tissue homeostasis after infection with influenza virus, *Nat. Immunol.*, 2011, **12**, 1045–1054.

52 B. Zeng, S. Shi, G. Ashworth, C. Dong, J. Liu and F. Xing, ILC3 function as a double-edged sword in inflammatory bowel diseases, *Cell Death Dis.*, 2019, **10**, 315.

53 X. Wang, N. Ota, P. Manzanillo, L. Kates, J. Zavala-Solorio, C. Eidenschenk, J. Zhang, J. Lesch, W. P. Lee, J. Ross, L. Diehl, N. van Bruggen, G. Kolumam and W. Ouyang, Interleukin-22 alleviates metabolic disorders and restores mucosal immunity in diabetes, *Nature*, 2014, **514**, 237–241.

54 J. Talbot, P. Hahn, L. Kroehling, H. Nguyen, D. Li and D. R. Littman, Feeding-dependent VIP neuron–ILC3 circuit regulates the intestinal barrier, *Nature*, 2020, **579**, 575–580.